Multi-year mosaics of Antarctic ice motion from satellite radar interferometry: 1995 to 2022

Eric Rignot[1,2], Jeremie Mouginot[1,3], Bernd Scheuchl[1], Seongsu Jeong[1]

[1]Dept. Earth System Science, University of California Irvine, Irvine, 92697 CA, USA.
[2]Jet Propulsion Laboratory, California Institute of Technology, Pasadena, 91107 CA, USA.
[3]University Grenoble Alpes, CNRS, INP, Grenoble IGE, Grenoble, France

Key Points:

- We present historical, continent-wide, mosaics of Antarctic motion using a suite of satellite sensors spanning the past 28 years.
- We report areas of accelerated ice flow stretching over 100 km's from the coast and the drainage of the entire Amundsen Sea sector.
- The observed, ongoing, detailed glacier changes will help constrain ice sheet numerical models in charge of reconstruction and projection.

Corresponding author: Eric Rignot, erignot@uci.edu

Abstract

Ice motion and ice boundary are critical information for ice sheet models that project ice evolution in a warming climate. We present four historical, continent-wide, maps of Antarctic ice motion and boundary for the time period 1995-2022. The results reveal no change in 2/3rd of the interior regions, block rotation and rift propagation at ice shelf fronts, and widespread glacier speedup that propagates from 10 to 100 km's inland. Speedup affects the entire drainage of the Amundsen Sea Embayment sector, in West Antarctica; the entire west coast of the Antarctic Peninsula down to GeorgeVI Ice Shelf; the east coast down to Larsen C Ice Shelf; Getz Ice Shelf, Hull and Land glaciers in West Antarctica; Matusevitch, Ninnis, Mertz and Denman glaciers, glaciers in Porpoise and Vincennes Bay, and Robert, Wilma and Rayner glaciers in Enderby Land, in East Antarctica. We attribute the changes to faster melting by warmer ocean waters.

Plain Language Summary

Ice velocity is a fundamental variable of glacier evolution that governs the transfer of mass from the ice sheets to the ocean. It is best measured from satellite platforms but long time series require combination of multiple satellite data of various performance levels and incomplete spatial coverage. We assembled the first set of continent-wide mosaics using 2 to 5 years of data in each period to maximize spatial coverage and detect changes in ice dynamics ice sheet wide. The results reveal no signal over 2/3rd of the interior but important changes at the coast concentrated along channels occupied by outlet glaciers. In the Amundsen Sea Embayment sector of West Antarctica, changes are pervasive over the entire drainage, which indicates that the coastal forcing from the ocean affects the entire ice sheet. The products reveal precise areas of rapid change in the West and East coasts of the Antarctica Peninsula, and in West and East Antarctica. These observations will help constrain ice sheet models in charge of reconstructing ice sheet past and projecting its evolution in a warming climate.

1 Introduction

The Antarctic Ice Sheet has been losing an increasing amount of mass in the last few decades, from 40±9 Gt/yr in 1979-1990, to 50±14 Gt/yr in 1989-2000, 166±18 Gt/yr in 1999-2009 and 252±26 Gt/yr in 2009-2017 (Rignot et al., 2019). During 2009-2017, the mass loss has been dominated by the Amundsen Sea Embayment (ASE) sector of West Antarctica (159±8 Gt/yr), the Wilkes Land in East Antarctica (51±13 Gt/yr) and West and Northeast Peninsula (42±5 Gt/yr). The mass loss is caused by changes in ice dynamics caused by the presence of warmer waters on ice shelves and glacier grounding lines, which reduces the resistance to glacier flow and increases the transport of ice from the continent to the ocean versus the amount required to keep the system in mass balance with the accumulation of snowfall over the drainage basins. Changes in speed measured at the grounding line, i.e. the transition boundary between grounded ice and ice floating in the ocean waters, combined with radar-derived measurements of ice thickness help constrain ice fluxes into ocean. It is however of importance to document how these changes affect the interior regions, how far inland, how fast, and where in Antarctica (Smith et al., 2020).

Mapping of ice velocity on the ground with theodolites and Global Positioning System has long been supplanted by satellite techniques, with records spanning from the early days of Corona/Argon (Li et al., 2017; Luo et al., 2021) in the 1960s, Landsat-1 (Rignot et al., 2019) in the 1970s, to the Synthetic-Aperture Radar (SAR) era of the 1990s with the European Earth Remote Sensing satellites 1 and 2 (ERS-1, 2), the 2000s with the European Envisat ASAR, the Canadian RADARSAT-1 and the Japanese Aerospace Exploration Agency (JAXA) Advanced Land Observing System (ALOS) PALSAR, and the mid 2010s with the European Union Copernicus Sentinel-1a/b series (S1a/b), combined with an improved time series of optical data from Landsat-8 Operational Land Imagery (OLI) and Sentinel-2 (S2).

We produced the first continental scale of ice sheet motion in Antarctica using ten years of data from multiple SAR satellites (ERS-1/2, RADARSAT-1, Envisat) (Rignot et al., 2011). The product was subsequently improved and extended in time by applying feature tracking of Landsat-8 optical data in the summer months and S1a/b SAR data year round using speckle tracking (Mouginot et al., 2017). The mapping accuracy was improved by one order of magnitude using the interferometric phase of SAR data instead of speckle tracking over 80% of Antarctica (Mouginot et al., 2019). With phase-only velocity, we detected the continuous speedup of Pine Island Glacier in the 1990s, on a monthly basis, to the limit of the ERS-1 data acquisition (Rignot et al., 2002). While the phase-only product cannot be updated routinely with the existing suite of satellite data and acquisition strategy, we can use the augmented suite of satellites to assemble speckle-tracking-based ice sheet wide mosaics over multiple years to maximize coverage and reduce data noise. In early 2024, phase-only products will become routinely available, on a monthly to submonthly basis, using the SAR data of the joint NASA Indian Space Research Organization (ISRO) NISAR mission (P. A. Rosen et al., 2016).

Here, we present historical multi-year, mosaicked data at the continental scale, along with a delineation of ice sheet boundaries for each time period: 1) 1995-2001; 2) 2007-2009; 3) 2014-2017; and 4) 2020-2022. As glaciers and ice shelves flow, the ice front positions migrate downstream until a calving event retreat them inland. Similarly, the grounding line may retreat (advance) with time in regions of rapid thinning (thickening) so that the transition boundary between ice and ocean must be updated. The grounding line boundary is critical to ice sheet modelers because it defines a transition region where ice no longer experiences basal resistance to flow. We discuss the product quality, the observed changes in speed over the four time periods, how they appear geographically, spatially, and temporally. We conclude on the importance of the results for ice sheet modeling and for detecting areas of ongoing changes in mass balance.

2 Data and Methods

Satellite data. The SAR data employed in this study have been acquired under the umbrella of the Polar Space Task Group (PSTG), which was established under the auspices of the World Meteorological Organization (WMO) Executive Council Panel of Experts on Polar Observations Research and Services. The group mandate was to provide coordination across International Space Agencies to facilitate acquisition and distribution of fundamental satellite datasets in support of polar science. Independently, the Landsat Science team independently provided the Landsat project at the United States Geological Survey with specific recommendations for ice sheet wide acquisitions for Landsat-8.

For the 1995-2001 map, we employ ERS-1/2 and RADARSAT-1 SAR data. ERS-1/2 operated from 1995 to 2018, on a 1 day cycle in 1995-1996 during the tandem mission and on a 35-day cycle otherwise, at the C-band frequency (5.6 cm wavelength), with a spatial resolution of 13 x 4 m (range x azimuth), north of 81°S. To process the data into a velocity map, we use speckle tracking (Michel & Rignot, 1999), the methodology in (Mouginot et al., 2012), and the mosaicking and calibration in (Mouginot et al., 2017). Speckle tracking uses sub-images of 64 x 256 pixels in range and azimuth and a search window of 16 x 16 pixels using the ampcor routine from ROI-PAC (P. Rosen et al., 2004). In our definition of annual maps, we use acquisitions spanning from 1 July to 30 June of the next year (centered on 1 January). We use this convention because previous SAR campaigns (2000-2010) from ALOS, Envisat, or RADARSAT-1/2 were mostly acquired between October and March.

RADARSAT-1 operated at C-band, on a 24-day cycle, at a resolution of 12 x 5 m, north of 77.5°S. The first interferometry data were collected in Sept. - Oct. 1997, in left looking mode (to map South Pole), during the Antarctic Mapping Mission 1 (AMM-1) (Jezek, 2002). Interferometry mapping was extended in right looking mode in Sept. to Nov. 2000 during the second Antarctic Mapping Mission (AMM-2) north of 80.1°S. AMM-2 data was used to make a mosaic of Antarctic velocity constrained by few calibration points. Here, we re-processed

the AMM-1/2 data into a new mosaic, with improved speckle tracking, data stacking, and automatic calibration which results in a higher velocity accuracy. Tracking uses averaging windows of 32 x 128 pixels in mode F6 (64 x 128 in mode F1) with search windows of 16 x 16 pixels (32 x 32 in mode F1). ERS-1/2 data is used in West Antarctica and the Antarctic Peninsula versus RADARSAT-1 elsewhere.

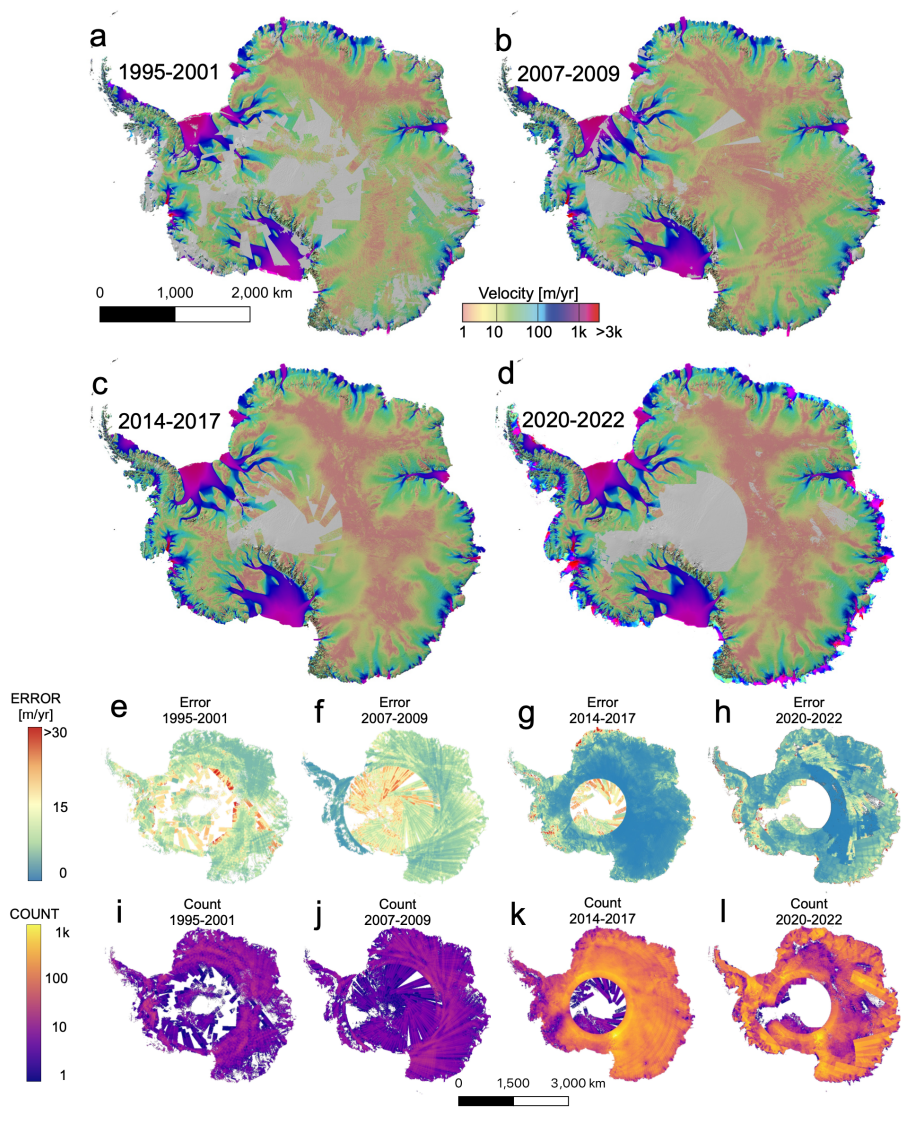

Figure 1: Multi-year mosaics of Antarctica ice motion from years: a) 1995-2001; b) 2007-2009; c) 2014-2017; and d) 2020-2022, color coded on a logarithmic scale from brown (low velocity) to yellow, green, blue and purple (high velocity) in m/yr. Projection is polar stereographic with a secant plane at 71°S (ESPG 3031). (e-h) Error in velocity in the order of a-d, and (i-l) pair count for each mosaic.

For the 2007-2009 map, we employed ERS-2 SAR, Envisat ASAR, ALOS PALSAR and RADARSAT-2. Envisat ASAR operated with a 35-day cycle, at the C-band frequency, with a spatial resolution of 13 x 4 m, north of 79.4°S. Envisat provided the first interferometric coast-to-coast tracks across Antarctica, which proved critical to produce a fully calibrated mosaic of East Antarctic motion. In mode IS2, we tracked sub-images 64 x 256 pixels with a search

window of 32 x 32 pixels. RADARSAT-2 operated at a 24-day repeat cycle at the C-band frequency and 12 x 5 m spacing in left looking mode, which allowed the first complete interferometric coverage of South Pole in 2009. Speckle tracking is the same as for RADARSAT-1.

Finally, ALOS PALSAR operated at the L-band frequency (24 cm wavelength), at a 46 day repeat cycle, with a resolution of 7 x 4 m, north of 77.5°S. We tracked sub-images 64 x 128 pixels in mode S2, 32 x 128 in mode S3, and 64 x 256 in mode S5, with search windows of 32 x 24 pixels. ALOS PALSAR provided superior coherence data at the L-band frequency but with more ionospheric noise than at C-band. These perturbations were corrected using an ionospheric removal algorithm for the phase data only (Liao et al., 2018). We tracked sub-images 128 x 256 pixels in mode FN1 with a search window of 64 x 64 pixels.

For the 2014-2017 and 2020-2022 maps, we employed S1-a/b, RADARSAT-2, and Landsat-8 data. S1a acquired data at a 12-day repeat cycle, at the C-band frequency (5.6 cm wavelength) in right looking mode, at a resolution of 12 x 43 m in Interferometric Wide Swath (IW) mode using Progressive Scans SAR (TOPS) technique, and north of 79°S. S1b was placed in a 6-day repeat mode with S1a in 2016. A TOPS IW swath is 250-km wide and is formed by combining 3 sub-swaths acquired in parallel. Each sub-swath consists of a series of bursts with their own doppler history. S1a is a right looking SAR, hence looking away from South Pole. The large gap around South Pole persists with sensors with right looking capability, except RADARSAT-2. For S1a/b, tracking is done with sub-images 192 x 48 pixels and search windows 32 x 8 pixels. After the launch of S1a/b, RADARSAT-2 focused on left looking mode to cover the interior of Antarctica.

For Landsat-8 (2013-2022), we use the panchromatic channel (Band 8) which has the highest spatial resolution (15 m) and covers a wavelength range between 0.5 and 0.68 μm north of 82.7°S. A 3 by 3 Sobel filter is applied in the horizontal directions to enhance small scale features and attenuate albedo changes. To assist feature tracking, we employ the a-priori displacements from prior velocity mappings. This step makes it possible to reduce the search area for pixel offsets at each location to windows about 4 by 4 pixels in size, with windows of 32 x 32 pixels, to reduce the computational load.

The gridded velocity data is distributed at 450 m in NetCDF format in Polar Stereographic (ESPG 3031) projection with true scale at 71°S. The data are accompanied by time-dependent shape files of the ice front and grounding line positions derived from SAR data, error maps for the velocity products, and amplitude imagery. The error is a weighted average of the nominal error in speed from each sensor (Mouginot et al., 2017).

Mosaicking and calibration. We use an automated calibration that takes advantage of ice velocity products from prior surveys (Mouginot et al., 2017). Offsets are first cleaned using median filtering. Afterward, a reference is extracted from prior surveys, converted into pixel displacement, and divided in 9 equally-sized sectors where reference displacements are sorted by magnitude. The 20% lowest speeds are used for calibration to minimize the impact of fast ice flow variation. The calibration is done by fitting the difference between the reference and offset map with a quadratic plane or a constant value for S1a/b and Landsat-8, respectively. To avoid long regions with high surface velocity, we perform the calibration on regions of concatenated data which includes multiple low to zero motion data. Geocoding use the BedMachine Antarctica Digital Elevation Model. The nominal errors in ice velocity are typically a few meters per year. The precision of data from a particular sensor depends on its resolution and its repeat cycle. Because sensors differ in both, their precision varies accordingly.

3 Results

The grounded ice sector of Antarctica decreased from 12,380,536 km^2 in 1995-2001 to 12,377,057 km^2 in 2007-2008, 12,373,831 km^2 in 2014-2017, and 12,369,049 for km^2 in 2020-2022, for a total loss of 3,479 km^2, 6,705 km^2, and 11,487^2, respectively, since 1995-2001 as a result of grounding line retreat. On average, the Antarctic grounded ice decreased by 425±20

km^2 per year in 1995-2022. The floating ice sector decreased from 1,602,920 km^2 to 1,565,061 km^2 in 2007-2008, 1,574,597 km^2 in 2014-2017, and 1,574,275 ^{2} in 2020-2022, or a net loss of 37,859 km^2, 28,324 km^2, and 28,644 km^2 as a result of calving (loss) and advance (gain). The average loss is 1,060±200 km^2, or twice faster than the rate of grounded ice loss. Ice shelves retreat faster than grounded ice.

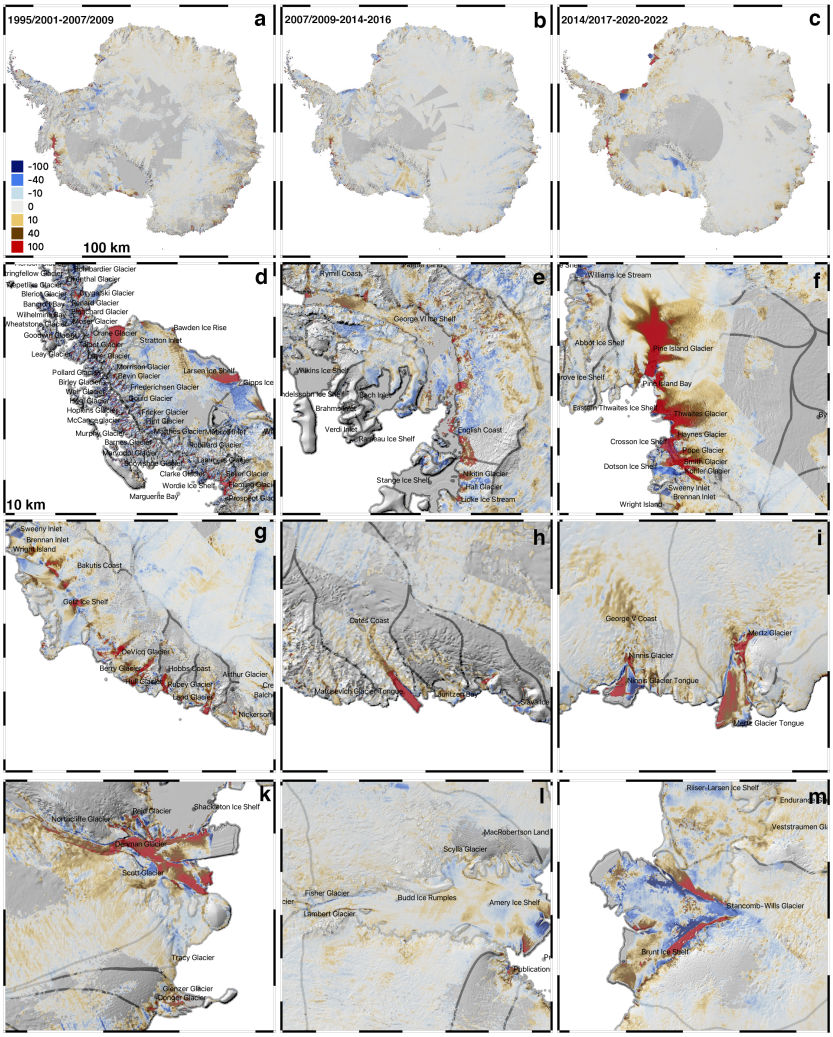

Figure 2: Multi-year mosaic of increase in speed for: a) 1995-2001 to 2007-2009; b) 2007-2009 to 2014-2017, and c) 2014-2017 to 2020-2022, with details for d) the Northern Antarctic Peninsula; e) the southern Antarctic Peninsula, f) ASE; g) Getz, Hull and Land, in West Antarctica; h) Matusevitch, i) Ninnis and Mertz, k) Denman, l) Amery Ice Shelf, and m) Stancomb Wills in East Antarctica with color coding from dark blue (< -100 m/yr) to red (>+100 m/yr) overlaid on the shaded-relief TanDEM-X digital elevation model of Antarctica. Areas with no velocity data are transparent. Panels d-e, h, k-m are the changes from 1995-2001 to 2014-2017; i is from 2007-2009 to 2014-2017; f-g from 1995-2001 to 2020-2022.

In 1995-2001, we mapped 75.4% of the ice sheet velocity and 74.6% of the floating ice velocity in area. The performance improved to 92.2%, 90.3%, and 84% for 2007-2009, 2014-2017, and 2020-2022, respectively, for grounded ice and 92.6%, 99.5%, and 99.9%, respectively for floating ice. Hence, the advent of new satellite missions has considerably reduced the duration needed for complete mapping, especially along the coast.

Over an area 888,320 km^2 in size in central East Antarctica with non-zero velocity for all four periods, the average speed is 4.1±3.6, 3.1±2.3, 2.5±1.5 m/yr, and 2.2±1.3m/yr, for the four periods 1995-2001, 2007-2009, 2014-2017, and 2020-2022, respectively. We detect changes in speed of 0.9±4.0 m/yr in 1995-2001 versus 2007-2009, 1.5±3.5 m/yr in 2007-2009 versus 2014-2017, and 0.3±1.2 m/yr in 2014-2017 versus 2020-2022. Hence, our noise level is 1.5 m/yr in 2007-2009, 2014-2017, and 2020-2022 versus 3.5 m/yr in 1995-2001. The last two time periods have seen a 10 x increase in the number of data available compared to prior periods (Figure 1). Over a contiguous area of 8,909,100 km^2 for which speed is non zero on all four periods, we find that 58% did not change at a detectable level (±3.5 m/yr) in 1995-2001 versus 2007-2009, 73% in 2007-2009 versus 2014-2017 (±, and 65% in 2014-2017 versus 2020-2022. Hence roughly 2/3rd of Antarctica does not change in speed at a detectable level.

On the large ice shelves, e.g. Ross, Filchner-Ronne, Amery, we eliminate changes in motion caused by the normal advance of ice fronts or their retreat due to calving events by using the ice masks for each time period. After applying this filter, we detect differential motion near many ice shelf fronts along sharp boundaries that coincide with active rift zones. A rift is an ice shelf fracture across the entire vertical column of the ice shelf. The rift is active if it propagates with time. On Filchner, ice on the northern side of two rifts parallel to the ice front, about 48 km (west) and 108 km (east) in length, respectively, and 68 km south of the ice front, increased their speed by 300 m/yr and 110 m/yr in 1995-2007 and -110 m/yr and +40 m/yr in 2007-2014. These velocity differential are precursor to calving events since the rifts are opening. On Amery, the divergence of the ice front as the ice shelf margins detach from the bay walls results in ice blocks rotating to the east on the east side and blocks rotating to the west on the west side, with differential motion of the order of 100 m/yr in opposite directions. On Ross, ice blocks in 1995-2001 which calved off parallel to the ice front between 1995 and 2007 experienced differential speeds on each side of the rift of up to +200 m/yr. Finally, ice blocks on the sides of major ice shelves, e.g. Ronne, experienced block rotation as ice moved past the margins of the bay walls (Larour et al., 2014).

More complex patterns are visible on Stancomb Wills and Denman in East Antarctica. On Stancomb-Wills, a rift 84 km in length, 18 km north of the grounding line between Stancomb Wills and Brunt Ice Shelf, sped up to 700 m/yr in 1995-2007 and the entire Brunt Ice Shelf sped up in 2014-2020. The pattern of ice motion has been attributed to the presence of active rifts and faults in the ice shelf (Larour et al., 2014). On Denman Glacier, the ice shelf and the glacier sped up starting in 1995-2007 and ongoing to present. The slower-moving ice shelf to the west of Denman, however, experienced enhanced friction along Denman ice tongue and sped up by 200 m/yr.

Of particular interest is the detection of the horizontal extent of glacier speed up in the interior regions. In West Antarctica, speed up is detected up to the ice divide of the northern branch of the drainage basin of Pine Island. In the southern branch, the satellite coverage is not sufficient but sparse results indicate that speed up occurs as well (Fig. 2). On Thwaites, the speed up propagates to the limit of our data, about 250 km south of the grounding line. Speed up affects most of the mapped drainages of Pope, Smith, and Kohler glaciers farther west. On Getz, the speed up propagates to within 80 km from the ice divide where data quality degrades. Similarly, speed up on DeVicq, Berry, Hull and Land glaciers propagate to their ice divides. In East Antarctica, on Denman, we detect speed up more than 400 km from the grounding line, along a deep trough. Conversely, we detect only a weak speed up for Totten and Frost/Holmes. Similarly, the speed up of Ninnis and Mertz is localized within 100-200 km of the coast.

In the Antarctic Peninsula, we detect a widespread acceleration of glaciers along the entire west coast, as reported previously in (Pritchard & Vaughan, 2007) for 1995-2001 and extended to 2017 in (Rignot et al., 2019). The speedup is ongoing and extends for each glacier from the ice fronts to the flanks of the central spine of the Antarctic Peninsula, i.e. more than 20-40 km inland, for all the marine-terminating glaciers. The glacier acceleration affects Fleming glacier to the south and all the major glaciers feeding into GeorgeVI Ice Shelf. The sig-

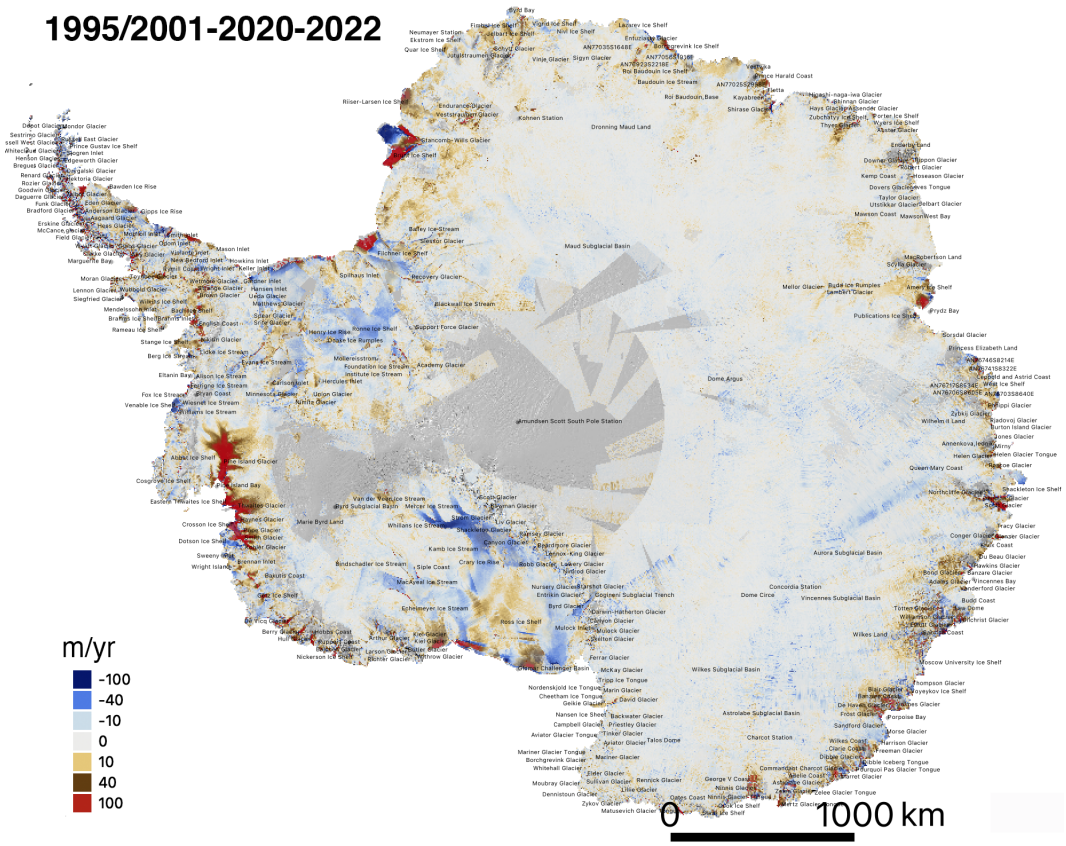

Figure 3: Multi-year mosaic of change in ice motion from 1995-2001 to 2020-2022, except for Getz and Georges VI where we use change from 2007-2009 to 2020-2022. Color coding is the same as Figure 2.

nal from the large (unnamed) glaciers flowing into GeorgeVI Ice Shelf Hogg et al. (2017) propagates to the limit of our data, within 10-20 km of the ice divide. A similar speed up is detected along the east coast of the Antarctic Peninsula starting north of Larsen A, in Trinity Peninsula, and extending into Larsen B and the northern half of Larsen C. The speed up is felt to the flanks of the central spine of the Antarctic Peninsula. Glacier speed up becomes more sporadic on Larsen D, typically at less than 40 m/yr, but in the case of glacier changes, we detect an acceleration propagating to the limit of our data, or within 10 km of the ice divides.

There are also notable examples of slow down. The most dominant slow down remains for the Siple Coast ice streams in West Antarctica (Thomas et al., 2013). The slow down of Mercer, Whillans, Van der Veen, and MacAyeal ice streams is detected 300-400 km inland of the grounding line and ongoing (Fig. 3). The magnitude of the slow down remains small, however, about 100 m/yr since 1995. In contrast, glaciers like Pine Island increased their speed by 2 km/yr since 1995. More surprisingly, we note the slow down of Venable Ice Shelf, in West Antarctica during the entire period and Shirase Glacier in East Antarctica.

4 Discussion

The mosaic products represent a massive data gathering, processing, and calibration effort of multi-sensor data. It took 5 years of data to cover 75% of Antarctica in 1995-2001 and 2 years in 2007-2009 to cover 90% of Antarctica. Since the launch of S1a/b and Landsat-8,

in addition to RADARSAT-2, a 90% coverage of Antarctica is possible to achieve within 2-3 years. All of these products were generated using a speckle tracking technique, which limits the precision of mapping to 2-3 m/yr. With a phase-only mapping using SAR data, as done over 80% of Antarctica (Mouginot et al., 2019), the noise level drops to 10-20 cm/yr, which makes it possible to map changes in speed 10 x times more precisely than herein, hence closer to the flanks of ice divides. Although phase-only data is difficult to use with S1a/b due to the mode of radar data acquisition, progress has been made using corrected phase data to map grounding lines (Mohajerani et al., 2021) and even ice velocity (Andersen et al., 2020), albeit only in one look direction since S1a/b only acquire descending tracks in Antarctica. ALOS PALSAR-2 data is difficult to access, data acquisition is limited to select areas in Antarctica, and combinations of ascending/descending tracks are not currently acquired. RADARSAT-2 data in left looking mode helps complete the phase mapping of areas closest to South Pole, but data acquisition competes with commercial activities, so the mission cannot be used to detect changes in speed on an annual basis. Lastly, Landsat-8 OLI is fundamentally limited in precision by feature tracking. There is no phase equivalent with optical data. The only possibility is to use longer temporal baselines (>1 year) at the cost of signal noise. The first opportunity for large-scale, continuous, phase mapping will be provided by the NISAR mission, at a 12-day repeat cycle, at the L-band frequency, with descending and ascending tracks over the entire Antarctic continent in left looking mode (P. A. Rosen et al., 2016).

With speckle tracking, we detect glacier speed up to our limit of detectability or the limit of data acquisition. The extent of the speed up is in ASE is consistent with the pattern of cumulative thinning observed from ICESat1-/ICESat-2 over the entire basin for 2003-2019 (Smith et al., 2020). The results indicate that changes in glacier flow propagate far inland, many 100 km's, to reach ice divides. On Getz Ice Shelf, we find a strong correlation between speedup and fast moving glaciers, which is only apparent with ICESat because of the large spacing between tracks. Flow acceleration is widespread but stronger on the west side of Getz. The West side is also more exposed to warm water (Jacobs et al., 2013) and the bathymetry favors a stronger circulation of ocean heat than on the east side (Millan et al., 2019). These results support the hypothesis that the ocean plays a major role in destabilizing the glaciers.

The speedup of Hull and Land glaciers is interesting because it extends the domain of ice flow acceleration farther west. These glaciers must also be affected by warm waters, but the presence of warm waters in front of them has not been discussed. Farther west, along Nickerson and Sulzberger ice shelves, glacier acceleration is weak to non existent, which suggests a limited influence of warm waters. This transition is consistent with a shallower seafloor on the continental shelf at that location (Arndt, 2013), which would block the access of subsurface warm waters to the continental shelf and the glaciers. Similarly, we do not detect speed up of the glaciers draining into Abbot Ice Shelf due to its shallow seafloor (Cochran et al., 2014).

In East Antarctica, the speedup of Denman Glacier propagates 400 km inland, along its deep trough, consistent the pattern in (Smith et al., 2020). But we we do not observe a large acceleration in the basin of Totten Glacier. Either our measurement error is too high or the glacier accelerated prior to the 1990s, therefore already out of balance in the 1990s. The latter explanation is supported by the estimated negative mass balance of the glacier in the 1990s (Rignot et al., 2019). Similarly, we do not detect speed up on Frost and Holmes glacier despite significant thinning, but the glaciers were also out of balance in the 1990s.

In the Antarctic Peninsula, our results are more detailed than ICESat and reveal that all marine-terminating glaciers are speeding up, including those flowing into Larsen C. The latter observation implies that basal melting of Larsen C ice shelf is likely to have increased, which was suggested as an possible lead explanation for the thinning of the ice shelf (Shepherd et al., 2003), however not confirmed by available ocean data (Nicholls et al., 2012).

The strong connection between coastal changes and interior regions in many parts of Antarctica has profound implications for ice sheet models. Models often report weak coupling between grounding lines and upstream areas, i.e. the effect of speed up is not expected to ex-

ceed a region of a few km (Mayer & Huybrechts, 1999). Matching the extent of the speed up and its timing will help constrain basal sliding and the type of sliding law to use (Joughin et al., 2019), determine the nature of the bed (weak till versus hard bedrock), evaluate the performance of various approximations, e.g. the MacAyeal shelfy stream model, the Blatter-Pattyn model, or a full Full-Stockes model (Morlighem et al., 2010) on how they balance stresses near the grounding line and beyond, and refine the treatment of ice ocean interaction at grounding lines (Seroussi & Morlighem, 2018). Model adjustments with these observations should considerably reduce the uncertainties of projections.

Many of the glaciers that speed up are already known to be close to warm waters, e.g. the west coast of the Antarctic Peninsula from Trinity Land to Fleming Glacier, GeorgeVI, Ferrigno, ASE, and Getz (Jenkins et al., 2016). Conversely, we lack ocean data on others, e.g. Hull and Land in West Antarctica, and Matusevitch, Ninnis, Frost, Rayner, Robert and Wilma in East Antarctica (Silvano et al., 2016). It would be of interest to address the issue of the presence of CDW near these glaciers. In West Antarctica, bathymetry coverage is sparse in front of Hull and Land glaciers, which should urgently be alleviated. A deep trough exist beneath Matusevitch (Morlighem et al., 2020), but there is no data to constrain the trough off shore. A deep trough exists beneath Ninnis that connects it to the deep, broad, submarine Wilkes Subglacial basin, but bathymetry coverage off shore is sparse, with no detail on the continental shelf. In the case of Frost and Holmes, the bed rises rapidly inland of the grounding line (Morlighem et al., 2020), so the potential for rapid retreat is lower than the other glaciers. Similarly, the glacier changes in Enderby Land, with Rayner, Robert and Wilma glaciers, also merit further investigation. These glaciers are not expected to be near warm waters a priori, but the bathymetry of the continental shelf is poorly known, yet the glaciers flow down a deep trough, hence are prone to rapid retreat. The troughs may extend off-shore since they were formed from basal erosion by former glacier advances (Allison et al., n.d.). If they retreat down these slopes, Enderby Land will become an archipelago. Finally, we note that Conger Ice Shelf, which collapsed in March 2022, was near warm CDW based on sea-mammal temperature data (Fig. S5 in (Brancato et al., 2020)). Conger has been retreating and speeding up steadily over the last 25 years, hence did not collapse only because of the warm 2022 summer event.

As our capability to map ice velocity increases in precision with phase-only mapping and more data acquisitions, we expect further progress in our ability to detect glacier changes, the extend of these changes inland, and better constrain ice sheet models over entire drainage basins. While speckle tracking has enabled spectacular progress in our mapping of glaciers and ice sheets over the past 28 years, it is essential to pursue these studies with phase-only data in the future to capture the full extent of the variability in ice flow in Antarctica.

5 Conclusions

In this study, we present the most comprehensive set of historical multi-year mosaic maps of Antarctica spanning from 1995 to 2022 using a speckle tracking approach. The products are accompanied by a delineation of ice boundaries, ice shelf fronts, and grounding lines, along with errors, of immediate interest and relevance to ice sheet models. The products have a nominal precision of a few meters per year, which allows the detection of changes far inland, although locally the errors may exceed these nominal values. Over most of interior Antarctica, we detect no change in speed. In many places, we are also not certain where changes stop propagating because our signal to noise ratio becomes too low. In the most important systems, e.g. ASE and Getz, the signal propagates to the ice divides, hence revealing a strong connection between grounding lines and the interior. In the Wilkes Land sector of East Antarctica, where changes in speed are lower, speckle tracking is not precise enough to delineate the full extent of speed up. This limitation will be lifted using phase-only data, e.g. with the launch of the NISAR mission in early 2024. We expect that these observations will provide additional constraints for ice sheet models in charge of reconstructing the past evolution of the ice sheet and predict its evolution in the coming century.

Acknowledgments

This work was performed in the Department of Earth System Science, University of California Irvine, and at Caltech's Jet Propulsion Laboratory under a contract with the National Aeronautics and Space Administration for the MEaSUREs program. We thank the space agencies and the PSTG who made the data available for this project.

6 Open Research

Mosaic products will be available at NSIDC as MEaSUREs product 0746 upon publication and also at https://datadryad.org/stash/share/63dLOLb8hC3iyCuEhMyLyYUeNH74n39k2SXa5WXE3Bc.

References

Allison, I., Frew, R., & Knight, I. (n.d.). Bedrock and ice surface topography of the coastal regions of Antarctica between 48^{o}E and 64^{o}E. *Polar Record*, *21(132)*, 241-252.

Andersen, J. K., Kusk, A., Boncori, J., Hvidberg, C. S., & Grinsted, A. (2020). Improved ice velocity measurements with Sentinel-1 TOPS Interferometry. *Rem. Sens.*, *12(12)*, 2014.

Arndt, J. e. a. (2013). The International Bathymetric Chart of the Southern Ocean Version 1.0 - A new bathymetric compilation covering circum-Antarctic waters. *Geophy. Res. Lett.*, *40*, 1-7.

Brancato, W., Rignot, E., Milillo, P., Morlighem, M., Scheuchl, B., Jeong, S., ... Prats-Iraola, P. (2020). Grounding line retreat of Denman Glacier, East Antarctica, measured with COSMO-SkyMed radar interferometry data. *Geophys. Res. Lett.*, *47*, e2019GL086291.

Cochran, J. R., Jacobs, S. S., Tinto, K. J., & Bell, R. E. (2014). Bathymetric and oceanic controls on Abbot Ice Shelf thickness and stability. *The Cryosphere,*, *8(3)*, 877–889.

Hogg, A., Shepherd, A., Cornford, S. L., Briggs, K. H., Gourmelen, N., Graham, J., ... Wuite, J. (2017). Increased ice flow in Western Palmer Land linked to ocean melting. *Geophy. Res. Lett.*, *44*, 4159-4167.

Jacobs, S., Giulivi, C., P., D., Rignot, E., Nitsche, F., & Mouginot, J. (2013). Getz Ice Shelf melting response to changes in ocean forcing. *J. Geophys. Res. Oceans*, *118*, 1-17.

Jenkins, A., Dutrieux, P., Jacobs, S., Steig, E., Gudmundsson, H., Smith, J., & Heywood, K. (2016). Decadal ocean forcing and Antarctica ice sheet response: lessons from the Amundsen Sea. *Oceanography*, *29(4)*, 58-69.

Jezek, K. C. (2002). Radarsat-1 antarctic mapping project: change-detection and surface velocity campaign. *Ann. Glaciol.*, 263-268.

Joughin, I., Smith, B., & Schoof, C. (2019). Regularized Coulomb friction laws for ice sheet sliding: Application to Pine Island Glacier, Antarctica. *Geophys. Res. Lett.*, *46*, 4764-4771.

Larour, E., Khazendar, A., Borstad, C. P., Seroussi, H., Morlighem, M., & Rignot, E. (2014). Representation of sharp rifts and faults mechanics in modeling ice shelf flow dynamics: Application to Brunt/Stancomb-Wills Ice Shelf, Antarctica. *J. Geophys. Res. Earth Surface*, *119*, 1918-1935.

Li, R., Ye, W., Qiao, G., Tong, X., Liu, S., Kong, F., & Ma, X. (2017). A new analytical method for estimating Antarctic ice flow in the 1960s from historical optical satellite imagery. *IEEE Trans. Geosci. Rem. Sens.*, *55*, 2771-2785.

Liao, H., Meyer, F. J., Scheuchl, B., Mouginot, J., Joughin, I., & Rignot, E. (2018). Ionospheric correction of InSAR data for accurate ice velocity measurement at polar regions. *Rem. Sens. Environ.*, *209*, 166-180.

Luo, S., Cheng, Y., Li, Z., Wang, Y., Wang, K., Wang, X., ... Li, R. (2021). Ice flow velocity mapping in East Antarctica using historical images from 1960s to 1980s: Recent progress. *Int. Arch. Photogramm. Remote Sens. Spatial Inf. Sci.*, *XLIII-B3*, 491-496.

Mayer, C., & Huybrechts, P. (1999). Ice-dynamic conditions across the grounding zone, Ekstromisen, East Antarctica. *J. Glaciol.*, *45(150)*, 384-393.

Michel, R., & Rignot, E. (1999). Flow of Glaciar Moreno, Argentina, from repeat-pass Shuttle Imaging Radar images: Comparison of the phase correlation method with radar interferometry. *J. Glaciol.*, *45(149)*, 93-100.

Millan, R., St-Laurent, P., Rignot, E., Morlighem, M., Mouginot, J., & Scheuchl, B. (2019). Constraining an ocean model Under Getz Ice Shelf, Antarctica, using a gravity-derived bathymetry. *Geophys. Res. Lett.*, *47*, e2019GL086522.

Mohajerani, Y., Jeong, S., Scheuchl, B., Velicogna, I., Rignot, E., & Milillo, P. (2021). Automatic delineation of glacier grounding lines in differential interferometric synthetic-aperture radar data using deep learning. *Nature Sci. Rep.*, *11*, 4992.

Morlighem, M., Rignot, E., Binder, T., Blankenship, D., Drews, R., Eagles, G., ... Young, D. A. (2020). Deep glacial troughs and stabilizing ridges unveiled beneath the margins of the Antarctic ice sheet. *Nat. Geosci.*, *13*(2), 132–137.

Morlighem, M., Rignot, E., Seroussi, H., Larour, E., Dhia, B., & Aubry, D. (2010). Spatial patterns of basal drag inferred using control methodsfrom a full-Stokes and simpler models for Pine Island Glacier, West Antarctica. *Geophys. Res. Lett.*, *37*, L14502.

Mouginot, J., Rignot, E., Scheuchl, B., & Millan, R. (2017). Comprehensive annual ice sheet velocity mapping using Landsat-8, Sentinel-1, and RADARSAT-2 data. *Remote Sensing*, *9*(4), 364.

Mouginot, J., Scheuchl, B., & Rignot, E. (2012). Mapping of ice motion in Antarctica using Synthetic-Aperture Radar Data. *Rem. Sens.*, *4*, 2753-2767.

Mouginot, J., Scheuchl, B., & Rignot, E. (2019). Continent-wide, interferometric SAR phase, mapping of Antarctic ice velocity. *Geophy. Res. Lett.*, *46*, 9710-9718.

Nicholls, K., Makinson, K., & Venables, E. (2012). Ocean circulation beneath Larsen C Ice Shelf, Antarctica from in situ observations. *Geophys. Res. Lett.*, *39*, L19608.

Pritchard, H. D., & Vaughan, D. (2007). Widespread acceleration of tidewater glaciers on the Antarctic Peninsula. *J. Geophys. Res.*, *112*, F03S29.

Rignot, E., Mouginot, J., & Scheuchl, B. (2011). Ice Flow of the Antarctic Ice Sheet. *Science*, *333*(6048), 1427-1430.

Rignot, E., Mouginot, J., Scheuchl, B., van den Broeke, M., van Wessem, M. J., & Morlighem, M. (2019). Four decades of Antarctic Ice Sheet mass balance from 1979 to 2017. *Proc. Natl. Acad. Sci.*, *116*(4), 1095–1103.

Rignot, E., Vaughan, D., Schmeltz, M., Dupont, T., & MacAyeal, D. (2002). Acceleration of pine island and thwaites glaciers, west antarctica. *Ann. Glaciol.*, *34*, 189-194.

Rosen, P., Hensley, S., Peltzer, G., & Simons, M. (2004). Updated repeat orbit interferometry package released. *Eos Trans. Amer. Geophys. Union*, *85*, 47.

Rosen, P. A., Hensley, S., Shaffer, S., Edelstein, W. N., Kim, Y., Kumar, R., ... Sagi, R. (2016). An update on the NASA-ISRO dual-frequency DBF SAR (NISAR) mission. *IEEE Trans. Geosci. Rem. Sens. Symp. (IGARSS)*, 2106-2108.

Seroussi, H., & Morlighem, M. (2018). Representation of basal melting at the grounding line in ice flow models. *The Cryosphere*, *12*, 3085-3096.

Shepherd, A., Wingham, D. J., Payne, T., & Skvarca, P. (2003). Larsen Ice Shelf has progressively thinned. *Science*, *302*, 856-859.

Silvano, A., Rintoul, S. R., & Herraiz-Borreguo, L. (2016). Ocean-Ice Shelf interaction in East Antarctica. *Oceanography*, *29(4)*, 100-113.

Smith, B., Fricker, H. A., Gardner, A. S., Medley, B., Nilsson, J., Paolo, F., ... Zwally, H. J. (2020). Pervasive ice sheet mass loss reflects competing ocean and atmosphere processes. *Science*, *368*(6496), 1239-1242.

Thomas, R., Scheuchl, B., Frederick, E., Harphold, R., Martin, C., & Rignot, E. (2013). Continued slowing of the Ross Ice Shelf and thickening of West Antarctic ice streams. *J. Glaciol.*, *59(217)*, 838-844.